S. DAOUD,[1] N. BIOUD[2]

[1] Faculté des Sciences et de la Technologie
(Université de Bordj Bou Arreridj, 34000, Algeria; e-mail: salah_daoud07@yahoo.fr)
[2] Laboratoire d'Optoélectronique & Composants
(Université Ferhat Abbes-Sétif, 19000, Algeria)

ANISOTROPY AND PRESSURE EFFECT ON THE ELASTIC AND MECHANICAL PROPERTIES OF (B3) BN

UDC 539

We present the results of ab initio calculations of the anisotropy and hydrostatic pressure effects on the elastic and mechanical properties of (B3) boron nitride, using the density functional perturbation theory (DFPT). The independent elastic and compliance constants, bulk and shear moduli, Zener anisotropy and Kleinman parameters, Cauchy and Born coefficients, Young modulus, and Poisson's ratio for directions within the important crystallographic planes of this compound under pressure are obtained. The crystal density, the longitudinal, transverse, and average sound velocities, and the Debye temperature under pressure are also studied. In the investigation of the stability criteria, the results showed a phase transition pressure from zinc blende to the rock-salt phase at about 4.54 Mbar, which is in good agreement with some available theoretical data reported in the literature and shows discrepancies with another ones.

Keywords: (B3) BN compound, elastic and mechanical properties, pressure and anisotropy effect, stability criteria.

1. Introduction

The mechanical properties of semiconductors often dictate fundamental limits on the fabrication and the packaging of modern semiconductor devices, so the study of these parameters is necessary and of high importance.

Boron nitride (BN) has useful physical properties such as the extreme hardness ∼4600 kg/mm^2, interesting optic and electronic characteristics (band gap = 7.5 eV, transmission ∼0.2–6 μm, refractive index $n \approx 2.117$), and important thermal characteristics (high melting point ∼3240 K, thermal conductivity ∼760 W/mK, thermal expansion ∼3.5(10^{-6} K), and heat capacity ∼0.513 J/gK) [1, 2]. The zinc blende (B3) structure of this compound was synthesized in 1957 [3].

First-principles computations and others theoretical methods predict that the cubic (B3) BN transforms to the rock-salt (B1) structure at pressures between 3.94 and 11.1 Mbar [4–15], well beyond the current limits of both experimental measurements and industrial needs. Recently, N. de Koker [14] used the first-principles molecular dynamics to evaluate the thermodynamics of zinc blende structured and liquid boron nitride at extreme conditions of temperatures and pressures and computed the melting curve up to 1 TPa.

In this study, we use the first-principles calculation to investigate the anisotropy and the hydrostatic pressure effect on the elastic and mechanical properties of the (B3) BN up to 4 Mbar. The independent elastic and compliance constants, bulk and shear moduli, the Zener anisotropy and Kleinman parameters, Cauchy and Born coefficients, and stability criteria under high pressure are obtained, using the density functional perturbation theory (DFPT) [17, 18]. The Young modulus and the Poisson's ratio for directions within the important crystallographic planes of (B3) BN compound are also determined, and finally, the evolution of the crystal density, the longitudinal, transverse, and average sound velocities, and the Debye temperature as a function of the hydrostatic pressure are studied.

The paper is organized as follows. In Section 2, we briefly describe the computational techniques used in this work.

Results and discussions are presented in Section 3. Finally, conclusions and some remarks are given in Section 4.

2. Computational Methods

The first-principles calculations were performed by using the density functional perturbation theory and implemented in the ABINIT code [19–21]. ABINIT code is a package, whose main program allows one to find the total energy, charge density, electronic structure and several other properties such as elastic, thermodynamic, optic, and piezoelectric ones of systems made of electrons and nuclei (molecules and periodic solids) within the density functional theory, using pseudopotentials and a plane-wave basis-set. It is a common project of the Universite Catholique de Louvain, Corning Inc., the Université de Liége, the Commissariat a l'Energie Atomique, Mitsubishi Chemical Corp., the Ecole Polytechnique Palaiseau, and other contributors.

We used the Teter and Pade parametrization [22] for LDA, and the Trouiller Martins scheme [23] to generate the norm-conserving nonlocal pseudopotentials to study the effect of hydrostatic pressure on the evolution of the crystal density.

The Kohn–Sham single-particle functions were expanded in the basis of a plane-wave set with a kinetic energy cut-off of 70 Hartree to obtain a convergence better than 10^{-6} Hartree for the total energy. Monkhorst–Pack special k-point grids [24] of 28 points were used for the integration over the Brillouin zone; this corresponds to the $(6 \times 6 \times 6)$ k-point mesh. Having obtained the self-consistent solutions of the Kohn–Sham equations, the elastic and mechanical properties were calculated within the framework of the self-consistent DFPT method [17, 18].

3. Results and Discussion

3.1. Elastic stiffness constants

On the macroscopic scale, the elastic properties of solid materials can be described by the use of the elastic moduli, which are related to the directional properties of a material [2]. The tensor relationships between stress (σ, a second-order tensor) and strain (e, a second-order tensor) are [2]:

$$\sigma_{ij} = C_{ijkl} e_{kl}, \tag{1}$$

$$e_{ij} = S_{ijkl} \sigma_{kl}, \tag{2}$$

where the fourth-rank tensors C_{ijkl} and S_{ijkl} are called the elastic stiffness C and the elastic compliance S, respectively. This is the tensor form of Hooke's law [2]. Each index (i, j, k, and l) has three values (x, y, and z); hence, the C and S tensors have 81 terms [2]. The stiffness and compliance tensors are usually written in a matrix notation made possible by the symmetry relationship of the stress and strain tensors [2].

The symmetry of a solid crystal reduces considerably the number of independent terms in the stiffness and compliance tensors (from 81 to 36) [2]. The usual notation for the reduced (matrix) notation form of the stiffness and compliance tensors is [2]:

$$\sigma_i = C_{ij} e_j, \tag{3}$$

$$e_i = S_{ij} \sigma_j, \tag{4}$$

where the indices, i and j, are an abbreviation of the ij or kl components (run from 1 to 6). Thus, the stiffness and compliance tensors are written as 6 by 6 matrices which can again be shown to be symmetric, given 21 independent terms [2]. The stiffness and compliance tensors are needed to completely describe the linear elastic properties of a crystal. Even a completely amorphous material has two independent constants that describe the relationship between stress and strain [2]. The number of independent elastic constants is reduced if the crystal possesses symmetry elements. In the important case of cubic crystals, there are only three independent stiffness constants (C_{11}, C_{12}, and C_{44}) [25].

There are different methods to obtain the elastic constant through the first principles. Nielsen and Martin [26] developed a method, using a strain-stress relation. Recently, Hamman *et al.* [27] developed a reduced coordinate metric tensor method for the linear response formulation of strain-type perturbations, which could be calculated by the DFPT method. The elastic constants reported in this article are obtained by the method used in [17, 18, 28], as implemented in the ABINIT code. The elastic stiffness tensor of a cubic structure has three independent components, namely C_{11}, C_{12}, and C_{44} in Young's notation.

For cubic crystals, the bulk modulus B is related to the elastic stiffness constants by the relation [29]

$$B = \left(\frac{C_{11} + 2C_{12}}{3} \right). \tag{5}$$

The obtained values of the elastic stiffness constants C_{ij} and the bulk modulus B of (B3) BN at various pressures are presented in Fig. 1.

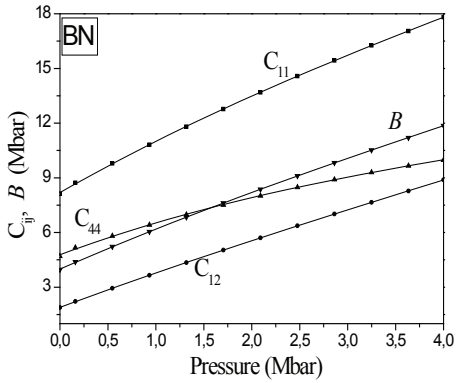

Fig. 1. Elastic stiffness constants C_{ij} and the bulk modulus B versus the hydrostatic pressure on (B3) BN

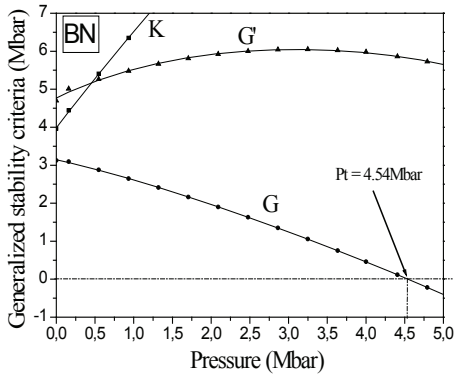

Fig. 2. Generalized stability criteria versus the hydrostatic pressure on (B3) BN compound

Transition pressure P_T on (B3) BN in comparison with the theoretical [4–15] data

	P_T (Mbar)
Our work	4.54
Other works	3.94 [4, 14], 6.24 [5], 8.50 [6], 10.88 [7], 5.55 [8], ∼5.061 [9], 10.25 [10], 5.00 [11], 9.45 [12], 11.1 [13], ∼10.212 [15]

As shown in this figure, we found that all the elastic stiffness constants increase gradually almost linearly with the hydrostatic pressure.

To study the stability of (B3) BN compound when a deformation is expressed in terms of the Lagrangian strain, the calculated values of the elastic constants under hydrostatic pressure were compared with the generalized stability criteria of Born [30], using the following relations [31, 32]:

$$K = \frac{1}{3}(C_{11} + 2C_{12} + P) > 0, \tag{6a}$$

$$G = \frac{1}{2}(C_{11} - C_{12} - 2P) > 0, \tag{6b}$$

$$G' = C_{44} - P > 0. \tag{6c}$$

The requirement of mechanical stability in a cubic crystal leads to the following restrictions on the elastic constants: $C_{11} - C_{12} > 0$, $C_{11} > 0$, $C_{44} > 0$, $C_{11} + 2C_{12} > 0$ [33]. The elastic constants at zero pressure obey these stability conditions, including the fact that C_{12} must be smaller than C_{11}. Our calculated elastic constants also obey the cubic stability conditions, meaning that $C_{12} < B < C_{11}$.

As a pressure is applied to (B3) BN compound, it transforms from the zinc blende phase into the site-ordered NaCl phase [8] or an amorphous phase proposed to exist between the zinc blende to rock-salt transition [4].

The variations of the generalized stability criteria of (B3) BN as a function of the hydrostatic pressure are presented in Fig. 2.

As shown in Fig. 2, we find that G decreases gradually with the increase in the hydrostatic pressure and vanishes at about 4.54 Mbar. Therefore, the phase transition occurs at 4.54 Mbar. This value of the transition pressure for (B3) BN is listed and compared with other theoretical [4–15] data in Table.

This value is in good agreement with the theoretical results in [9, 11] and it deviates by 10.29% and 9.2%, respectively.

It is clearly seen that our result (4.54 Mbar) is substantially lower than the value of 11.1 Mbar obtained in [13], by using the thermodynamic instability total energy calculations method, with the LDA pseudopotential approach and the Wigner interpolation formula [34] for the exchange and correlation functional.

These are the kinetic criteria, under which the structure becomes mechanically unstable, as opposed to the thermodynamic instability used in total energy calculations (usually by using the equality of the enthalpies of different phases), which makes no reference to a transition route [35]. The resulting thermodynamic transition pressure will be a lower limit to the observed transition [35]. The elastic criteria prescribe a particular homogeneous deformation as the reaction path, the real path is probably more complex, and,

hence, the elastic criteria give an upper limit on the transition pressure [35].

Usually, the elastic properties of materials are expressed in terms of engineering (or technical) moduli: shear modulus G and the bulk modulus B [2]. For cubic monocrystals, the shear modulus G is related to the elastic stiffness constants by the relation [29]

$$G = (C_{11} - C_{12})/2. \tag{7}$$

For the cubic polycrystals, the shear modulus is the average of two different results representing upper and lower bounds. It is a property of the isotropic polycrystalline aggregate, and it is not easy to estimate, therefore, the two bounds (in the framework of the Voigt–Reuss–Hill (VRH) approximation). The shear modulus G_{VRH} is given by the expression [36, 37]

$$G_{\mathrm{VRH}} = \left(\frac{G_{\mathrm{V}} + G_{\mathrm{R}}}{2}\right). \tag{8}$$

Here, G_{R} is the Reuss modulus given by

$$G_{\mathrm{R}} = \frac{5(C_{11} - C_{12})C_{44}}{4C_{44} + 3(\mathrm{C}_{11} - C_{12})}, \tag{9}$$

and G_{V} is the Voigt modulus defined as

$$G_{\mathrm{V}} = \frac{(3C_{44} + C_{11} - C_{12})}{5}. \tag{10}$$

The hydrostatic pressure effect on the variation of the Reuss modulus, Voigt modulus, and shear modulus for this compound is presented in Fig. 3.

For a cubic crystal material, the Zener anisotropy parameter Z is also related to the elastic stiffness constants C_{ij} by the relation [29, 38]

$$Z = \frac{2C_{44}}{(C_{11} - C_{12})}. \tag{11}$$

If $Z < 1$, the crystal is stiffest along $\langle 100 \rangle$ cube axes, and, when $Z > 1$, it is stiffest along the $\langle 111 \rangle$ body diagonals [39].

The Kleinman parameter is an important parameter describing the relative position of the cation and anion sublattices. It is given by the relation [36]

$$\xi = \frac{C_{11} + 8C_{12}}{7C_{11} + 2C_{12}}. \tag{12}$$

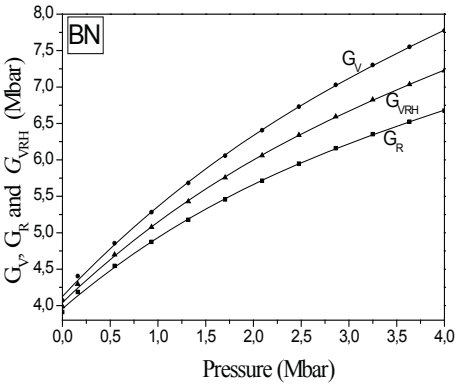

Fig. 3. Reuss modulus G_{R}, Voigt modulus G_{V}, and the shear modulus G_{VRH} versus the hydrostatic pressure

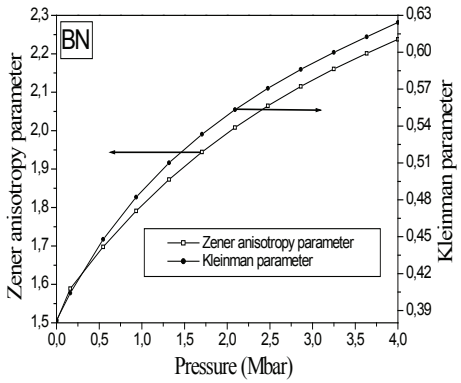

Fig. 4. Zener anisotropy parameter Z and Kleinman parameter ξ versus the pressure

The hydrostatic pressure effect on variations of the Zener anisotropy parameter Z and the Kleinman parameter ξ for this compound is presented in Fig. 4.

As shown in Fig. 4, both the Zener anisotropy parameter and the Kleinman parameter increase gradually with the hydrostatic pressure. The former takes the value 1.50 at $P = 0$ and reaches the value 2.24 at 4 Mbar, and the latter takes the value 0.38 at $P = 0$ and reaches the value 0.62 at 4 Mbar.

For the cubic crystals, the Cauchy and Born coefficients (C_{a} and B_o), are also related respectively to the elastic stiffness constants by the following relations [25]:

$$C_{\mathrm{a}} = \frac{C_{11}}{C_{44}}, \tag{13}$$

$$B_O = \frac{(C_{11} + C_{12})^2}{4C_{11}\,(C_{11} - C_{44})}. \tag{14}$$

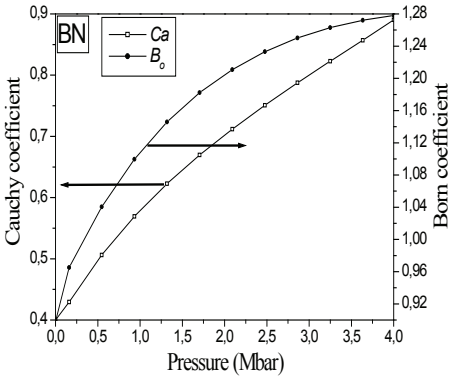

Fig. 5. Cauchy and Born coefficients versus the hydrostatic pressure

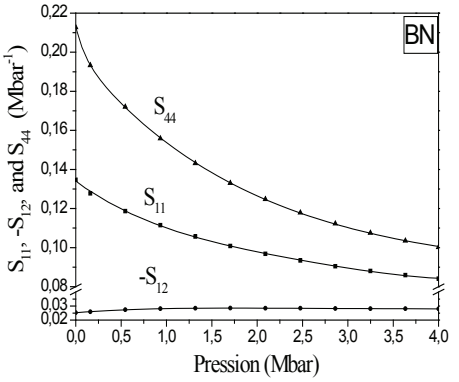

Fig. 6. Compliance constants S_{ij} versus the hydrostatic pressure

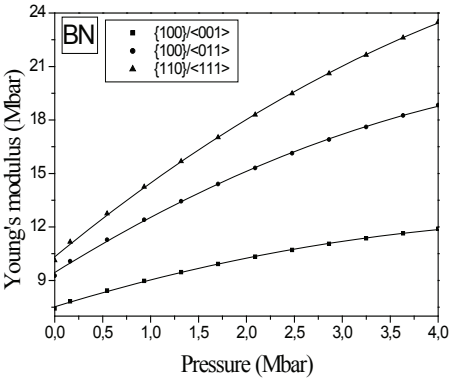

Fig. 7. Young modulus versus the hydrostatic pressure

The hydrostatic pressure effect on the variation of the Cauchy and Born coefficients is presented in Fig. 5. As shown in this figure, both C_a and B_o increase with hydrostatic pressure.

3.2. Compliance Constants

The elastic compliance tensor $[S]$, which has the same form as $[C]$, is connected reciprocally with the tensor $[C]$ through Hooke's relation.

The explicit relations for the component S_{ij} in terms of C_{ij} can be given by [25]

$$S_{11} = (C_{11} + C_{12})/[(C_{11} - C_{12})(C_{11} + 2C_{12})], \quad (15a)$$

$$S_{12} = (-C_{12})/[(C_{11} - C_{12})(C_{11} + 2C_{12})], \quad (15b)$$

$$S_{44} = 1/C_{44}. \quad (15c)$$

The obtained values of the compliance constants S_{ij} of (B3) BN at various pressures are presented in Fig. 6.

As shown in Fig. 6, both the compliance constants S_{11} and S_{44} decrease with increasing the hydrostatic pressure, whereas the constant S_{12} is almost invariant with the variation of the hydrostatic pressure.

3.3. Young modulus and Poisson's ratio

The Young modulus is defined as the ratio of the longitudinal tension to the longitudinal strain under tension, a quantity which is anisotropic for all crystal classes [2, 40], but is isotropic for amorphous materials [2]. Therefore, the engineering moduli only accurately describe the elastic behavior of isotropic materials. The engineering moduli also approximately describe the elastic behavior of polycrystalline materials [2].

The modulus Y for an arbitrary crystallographic direction m can now be given by [25, 41, 42]

$$1/Y = S_{11} - 2\,(S_{11} - S_{12} - 0.5S_{44}) \times$$

$$\times \left(m_1^2 m_2^2 + m_2^2 m_3^2 + m_1^2 m_3^2\right), \quad (16)$$

where the S_{ij} values are the elastic compliance constants, and m_i are the direction cosines.

The obtained values of the Young modulus at different pressures for important directions are presented in Fig. 7.

As shown in this figure, all the curves of the Young modulus increase with the pressure.

Poisson's ratio P also varies with orientation. If a longitudinal stress in the direction m and the transverse strain along the orthogonal direction n are under consideration, then the ratio P can be given by [25, 40, 41]

$P =$

$$= -\frac{\left[S_{12}+(S_{11}-S_{12}-0.5S_{44})(m_1^2n_1^2+m_2^2n_2^2+m_3^2n_3^2)\right]}{\left[S-2(S_{11}-S_{12}-0.5S_{44})(m_1^2m_2^2+m_2^2m_3^2+m_1^2m_3^2)\right]}. \quad (17)$$

The obtained values of P at different pressures up to 4 Mbar for important directions are presented in Fig. 8.

3.4. Crystal density, sound velocity, and Debye temperature

The crystal density g is related to the atomic arrangement and the corresponding electron density map [25]. There are four molecules in a unit cell of the zinc blende (B3) lattice (Fig. 9). If the accurate lattice constant is available, the calculation of g gives, in principle, a good reliable value.

The X-ray crystal density g can be simply written in terms of d_{M} as [25]

$$g = \frac{M d_{\mathrm{M}}}{N_{\mathrm{A}}} = \frac{4M}{N_{\mathrm{A}}V}, \quad (18)$$

where M is the molecular weight ($M = 24.818$ amu), N_{A} is the Avogadro constant ($N_{\mathrm{A}} = 6.022 \times 10^{23}$ mol^{-1}), V is the volume of a unit cell, and d_{M} is the molecular density. For the zinc-blende-type semiconductors, $d_{\mathrm{M}} = 4/a^3$ [25].

The calculated crystal density versus the hydrostatic pressure is plotted in Fig. 10.

The crystal density at zero pressure is equal to 3.545 g/cm^3, this value is in good agreement with the available theoretical value ($g = 3.488$ g/cm^3 [25]).

If the crystal density g and the stiffness constant C_{ij} of a solid are known, one can calculate the bulk sound velocity v from the general relation [25]

$$v = \left(\frac{C_{ij}}{g}\right)^{1/2}. \quad (19)$$

The average sound velocity is given by [38]

$$v_{\mathrm{m}} = \left[\frac{1}{3}\left(\frac{2}{v_{\mathrm{t}}^3} + \frac{1}{v_{\mathrm{l}}^3}\right)\right]^{-1/3}, \quad (20)$$

where v_{l} and v_{t} are the longitudinal and transverse sound velocities obtained by using the shear modulus G, bulk modulus B, and density g from Navier's equation [38]

$$v_{\mathrm{l}} = \left(\frac{3B+4G}{3g}\right)^{1/2}, \quad v_{\mathrm{t}} = \left(\frac{G}{g}\right)^{1/2}. \quad (21)$$

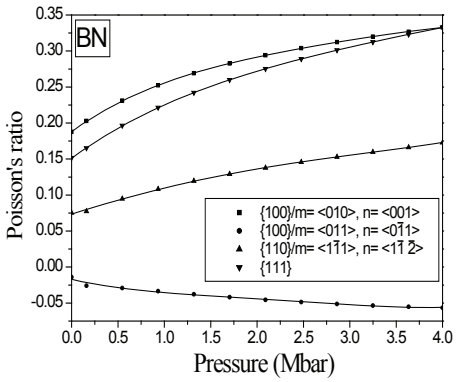

Fig. 8. Poisson's ratio versus the hydrostatic pressure

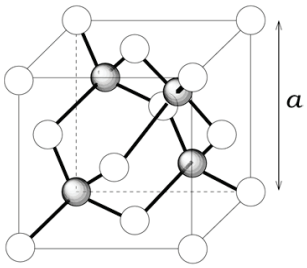

Fig. 9. Unit cell of the (B3) lattice, a is the lattice constant

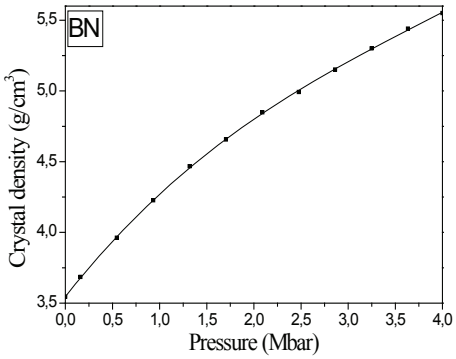

Fig. 10. Crystal density versus the hydrostatic pressure

The calculated longitudinal (v_{l}), transverse (v_{t}), and average (v_{m}) sound velocities versus the hydrostatic pressure on BN are plotted in Fig. 11. As shown in this figure, the sound velocity increases with the hydrostatic pressure up to 4 Mbar.

One of the standard methods to calculate the Debye temperature (θ_{D}) uses data on the elastic constants, since θ_{D} can be estimated in terms of the average sound velocity v_{m} [38]:

$$\theta_{\mathrm{D}} = \frac{h}{k_{\mathrm{B}}}\left(3/4\pi V_{\mathrm{a}}\right)^{1/3} \nu_{\mathrm{m}}. \quad (22)$$

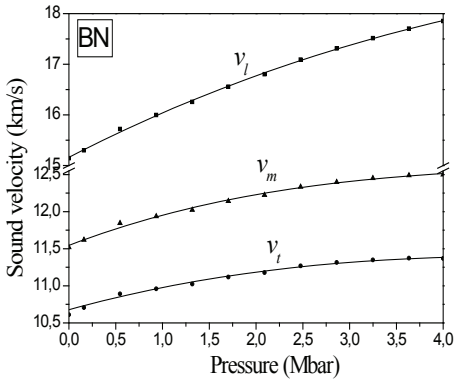

Fig. 11. Longitudinal, transverse, and average sound velocities in BN versus the hydrostatic pressure

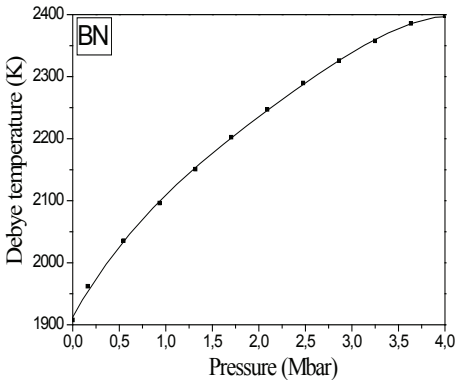

Fig. 12. Debye temperature versus the pressure

Here, h is the Planck constant, k_{B} is the Boltzmann constant, and V_{a} is the atomic volume.

At low temperatures, the vibrational excitation arises solely from acoustic modes. Hence, at low temperatures, the Debye temperature calculated from the elastic constants is the same as that determined from specific heat measurements.

The variation of the Debye temperature θ_{D} versus the increasing hydrostatic pressure P of the BN is plotted in Fig. 12.

As shown in this figure, θ_{D} increases with the hydrostatic pressure to reach a value of 2400 K at $P = 4$ Mbar.

The Debye temperature of polycrystals of the (B3) BN compound calculated at zero pressure is equal to 1907.6 K, which is in excellent agreement with data available in the literature [43]. It deviates slightly from the value 1987 K obtained with the use of the second-order elastic constants C_{ij} and other mechanical parameters.

4. Conclusions

The conclusions of this study to be summarized as follows:

The effect of the hydrostatic pressure on the elastic stiffness constants of this material is revealed in that all these elastic constants increase almost linearly with the pressure, except for the compliance constants, which decrease with the increase in the hydrostatic pressure with a negative sign for the S_{12}.

The hydrostatic pressure effects on variations of the shear and bulk moduli, Zener anisotropy and Kleinman parameters, Cauchy and Born coefficients, crystal density, longitudinal, transverse, and average sound velocities, and Debye temperature are also studied.

The obtained values of the compliance constants S_{ij} were used to predict the anisotropy effect on the two mechanical parameters: Young modulus Y and Poisson's ratio P.

In the investigation of the stability criteria, the results showed a phase transition pressure from zinc blende to the rock-salt (or amorphous) phase at about 4.54 Mbar, which is in good agreement with some available theoretical data reported in the literature and shows discrepancies with another ones.

1. M.J. Weber, *Handbook of Optical Materials* (CRC Press, Boca Raton, 2003).
2. W.J. Tropf, M.F. Thomas, and T.J. Harris, *Properties of Crystals and Glasses, Handbook of Optics* (McGraw-Hill, New York, 2004), Vol. IV.
3. R.H. Wentorf, J. Chem. Phys. **26**, 956 (1957).
4. Z.Y. Mijbil, J. of Bababylon Univ. **18**, 1686 (2010).
5. F. El Haj Hassan, H. Akbarzadeh, and M. Zoaeter, J. Phys. Condens.-Mat. **16**, 293 (2004).
6. N.E. Christensen and I. Gorczyca, Phys. Rev. B **50**, 4397 (1994).
7. S. Cui, W. Feng, H. Hu, and Z. Feng, Central Eur. J. Phys. **8**, 628 (2009).
8. A. Zaoui and F. El Haj Hassan, J. Phys. Condens.-Mat. **13**, 253 (2001).
9. S. Saib and N. Bouarissa, J. Alloy. Compd. **448**, 11 (2008).
10. I. Gorczyca and N.E. Christensen, Physica B **185**, 410 (1993).
11. Haneen Yousef Saeed Shalash, *Thesis of Master of Science, An-Najah-National University* (Palestine, 2009).
12. F. EL Haj Hassan, *These de Doctorat, Universite de Metz* (France, 2000).
13. R.M. Wentzcovitch, M.L. Cohen, and P.K. Lam, Phys. Rev. B **36**, 6058 (1987).

14. W. Sekkal, B. Bouhafs, H. Aourag, and M. Certier, J. Phys: Condens. Matter **10**, 4975 (1998).
15. Z.Y. Mijbil, Chem. Mater. Res. **2**(4), 30 (2012).
16. N. de Koker, J. Phys: Condens. Matter **24**, 055401 (2012).
17. S. Baroni, P. Giannozzi, and A. Testa, Phys. Rev. **58**, 1861 (1987).
18. P. Giannozzi, S. de Gironcoli, P. Pavone, and S. Baroni, Phys. Rev. B **43**, 7231 (1991).
19. X. Gonze, J.M. Beuken, R. Caracas *et al.*, Comp. Mat. Sci. **25**, 478 (2002).
20. X. Gonze, G.M. Rignanese, M. Verstraete *et al.*, Zeit. Kristallogr. **220**, 558 (2005).
21. S. Goedecker, SIAM J. Sci. Comput. **18**, 1605 (1997).
22. J.P. Perdew, K. Burke, and M. Ernzerhof, Phys. Rev. Lett. **77**, 3865 (1996).
23. N. Troullier and J.L. Martins, Phys. Rev. B **43**, 1993 (1991).
24. H.J. Monkhorst and J.D. Pack, Phys. Rev. B **13**, 5189 (1976).
25. S. Adachi, *Physical Properties of III-V Semiconductor Compounds* (Wiley, New York, 1992).
26. O.H. Nielsen and R.M. Martin, Phys. Rev. B **32**, 3792 (1985).
27. D.R. Hamman, X. Wu, K.M. Rabe, and D. Vanderbilt, Phys. Rev. B **71**, 035117 (2005).
28. A. Benamrani, K. Kassali, and Kh. Bouamama, High Pressure Res. **30** (1), 207 (2010).
29. S. Singh and M. Sarwan, J. Optoelectron. Adv. M. **12** (10), 2106 (2010).
30. J. Wang and S.Yip, Phys. Rev. Lett. **71**, 4182 (1993).
31. K. Bouamama, N. Lebgaa, and K. Kassali, High Pressure Res. **25**, 217 (2005).
32. S. Daoud, K. Loucif, N. Bioud, N. Lebgaa, and L. Belagraa, Pramana J. Phys. **79**, 95 (2012).
33. M. Born and K. Huang, *Dynamical Theory of Crystal Lattices* (Clarendon, Oxford, 1954).
34. E. Wigner, Trans. Faraday Soc. **34**, 678 (1938).
35. G.J. Ackland, Rep. Progr. Phys. **64**, 483 (2001); G.J. Ackland, *High Pressure Phases of Group IV and III-V Semiconductors* (Univ. of Edinburgh, Edinburgh, 1992).
36. H. Zhao, A. Chang, and Y. Wang, Physica B **404**, 2192 (2009).
37. L. Bing, L.R. Feng, Y. Yong, and Y.X. Dong, Chin. Phys. B **19**, 076201 (2010).
38. Z. Charifi, H. Baaziz, Y. Saeed, Ali Hussain Reshak, and F. Soltani, Phys. Status Solidi B **249**, 18 (2012).
39. R.E. Newnham, *Properties of Materials: Anisotropy, Symmetry, Structure* (Oxford Univ. Press, USA, 2005).
40. W.A. Brantley, J. Appl. Phys. **44**, 534 (1973).
41. M.A. Hopcroft, W.D. Nix, and T.W. Kenny, J. Microelectromech. S **19**, 229 (2010).
42. J.F. Nye, *Physical Properties of Crystals: Their Representation by Tensors and Matrices* (Oxford Univ. Press, Oxford, 1985).
43. H. Siethoff and K. Ahlborn, Phys. Status Solidi B **190**, 179 (1995).

Received 22.04.13

С. Дауд, Н. Біуд

ВПЛИВ АНІЗОТРОПІЇ ТА ТИСКУ НА ПРУЖНІ І МЕХАНІЧНІ ВЛАСТИВОСТІ НІТРИДУ БОРУ (B3)

Р е з ю м е

Представлено результати розрахунків з перших принципів впливу анізотропії та тиску на пружні і механічні властивості нітриду бору (B3) в рамках теорії збурень функціонала густини. Отримано незалежні константи пружності і податливості, об'ємний модуль, модуль зсуву, параметр анізотропії Зенера, параметр Клейнмана, коефіцієнти Коші і Борна, модуль Юнга і коефіцієнт Пуассона для напрямів в основних кристалографічних площинах при впливі тиску. Досліджено залежності густини кристала, поздовжньої, поперечної і середньої швидкостей звуку і температури Дебая від тиску. При вивченні критеріїв стабільності виявлено фазовий перехід при тиску близько 4,54 Мбар з фази сфалерита в фазу кам'яної солі в доброму узгодженні з теоретичними даними з літератури і в суперечності з деякими іншими результатами.

С. Дауд, Н. Биуд

ВОЗДЕЙСТВИЕ АНИЗОТРОПИИ И ДАВЛЕНИЯ НА УПРУГИЕ И МЕХАНИЧЕСКИЕ СВОЙСТВА НИТРИДА БОРА (B3)

Р е з ю м е

Представлены результаты расчетов из первых принципов воздействия анизотропии и давления на упругие и механические свойства нитрида бора (B3) в рамках теории возмущений функционала плотности. Получены независимые константы упругости и податливости, объемный модуль, модуль сдвига, параметр анизотропии Зенера, параметр Клейнмана, коэффициенты Коши и Борна, модуль Юнга и коэффициент Пуассона для направлений в основных кристаллографических плоскостях при воздействии давления. Исследованы зависимости плотности кристалла, продольной, поперечной и средней скоростей звука и температуры Дебая от давления. При изучении критериев стабильности обнаружен фазовый переход при давлении около 4,54 Мбар из фазы сфалерита в фазу каменной соли в хорошем согласии с теоретическими данными из литературы и в противоречии с некоторыми другими результатами.